Green Chemistry

Accepted Manuscript

ROYAL SOCIETY OF CHEMISTRY

rsc.li/green-chem

View Article Online
DOI: 10.1039/C7GC01405H

Benign-by-design preparation of iron oxides/humins catalytic nanocomposites

Layla Filiciotto[a], Alina M. Balu[a], Antonio A. Romero[a], Enrique Rodríguez-Castellón[b], Jan C. van der Waal[c], Rafael Luque[a]*

[a]*Departamento de Química Orgánica, Universidad de Córdoba, Edificio Marie Curie (C-3), Ctra Nnal IV-A, Km 396,E14014 Córdoba, España, e-mail: q62alsor@uco.es*

[b]*Departamento de Química Inorgánica, Cristalografía y Mineralogía, Facultad de Ciencias, Universidad de Málaga, 29071 Málaga, España.*

[c]*Avantium Chemicals B.V., Zekeringstraat 29, 1014 BV Amsterdam, The Netherlands*

Abstract

The current acid-catalyzed conversion of biomass feedstocks yields substantial quantities of undesired by-products called humins, for which applications has yet to be found. This work aims to provide a starting point for humins valorisation via preparation of humin-based iron oxide catalytic nanocomposites from humins and thermally treated humins (foams) via solvent-free methodologies including ball milling and thermal degradation. The prepared materials were found to be active in the microwave-assisted selective oxidation of isoeugenol (conversions > 87%) to vanillin, proving the feasibility to use humin by-products as template/composite materials.

Introduction

World's continuous scientific improvement, alongside the depletion of fossil feedstocks, calls upon the investigation of new sustainable processes using renewable sources. The synthesis of new active catalytic materials will play an important role achieving this. Recent progress in biorefinery concepts leads the way in the production of platform chemicals from biomass as widely available renewable resource[1-6]. As a matter of fact, Avantium's YXY technology has announced plams to build a 50 kta plant to convert biomass-derived sugars into platform chemicals (*e.g.* furanics, levulinics) for the synthesis of bio-plastics and fuels. In particular, the polymerization of YXY furanic building block (FuranDiCarboxylic Acid, FDCA) with mono-ethylene glycol gives

View Article Online
DOI: 10.1039/C7GC01405H

rise to PEF (polyethyene furanoate), a polyester with superior barrier and thermal properties compared to extensively used PET (polyethylene terephthalate)[7]. However, the current conversion of plant-based stocks yields parallel substantial quantities of insoluble and intractable, black, sticky substances usually referred to as humins[8-10]. These humins are generally considered to comprise of a series of oligomers (270-650 g/mol) containing furanic, sugars, and aromatic moieties linked by mainly short aliphatic chains. Additionally, they include at a smaller extent acetal or ether bonds, deriving from random condensation reactions of the main bio-derived molecules formed during the acid-catalysed dehydration of sugars (*e.g.* HMF, furfural, carbohydrates, levulinates, Scheme 1)[11,12]. Functional groups including carboxylic, ketone, aldehyde and/or hydroxyl are shown by bulk analysis in the final structure of humin by-products, thus the presence of superficial oxygen functionalities are expected[13]. Typical elemental composition of humins is found to be in the order of *ca.* 65wt% carbon, 5wt% hydrogen, and 30wt% oxygen[14]. Recently, Bruijnincx et al.[15] reported the quantification and classification of carbonyls groups for industrial humins and lignin, finding a higher contents of both aliphatic and conjugated carbonyl groups in the humins sample (6.6 wt%) compared to Alcell (3.3 wt%) and Indulin Kraft (1.7 wt%) lignins. The significant presence of organic functional groups and the broad range of molecular weights suggest a wide applicability of humin by-products as stabilizers, templates and combustible agents, to name a few. It could be hypothesised that the residual oxygen functionalities could play an important role as catalytic active sites for redox and oxidation reactions, in a similar fashion to graphene oxide[16].

Current research on humins is mainly focused on limiting the production of these compounds, so far considered waste[17]. Nonetheless, a few humin valorisation studies have been carried out, *e.g.* gasification to syngas[18], hydrocracking and hydrodeoxygenation to hydrocarburic molecules[19] or as a resin additive as shown by the improved mechanical properties of PFA(perfluoroalkoxy alkanes)/humins composite[20]. The limited number of valorisation studies, so far promted to research the possibilities of employing humins as a material additive or a platform chemical. Alternatively, this study has been aimed to provide an alternative valorisation of humins by-products as material composite/template in the synthesis of active catalytic materials.

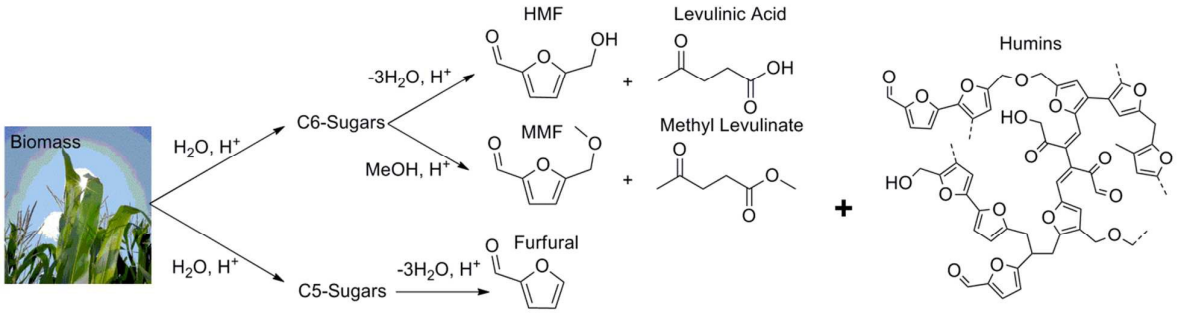

View Article Online
DOI: 10.1039/C7GC01405H

Scheme 1. Pathways formation of humin by-products.

Selective oxidative cleavage of hydrocarbons is one of the most relevant reactions in organic synthesis, finding applications in the conversion of both fossil and renewable feedstocks to industrial bulk and fine chemicals[21-25]. Traditional approaches often resort to toxic and/or environmentally harmful oxidants, *e.g.* ozone, permanganate, dichromate, or hypervalent iodine reagents[27-32], which also often lead to extremely high E-factors (*i.e.* the ratio of mass of waste products over the mass of the desired compound)[26]. Thanks to increasingly stringent environmental policies, but also an increased awareness of the scientific community in terms of sustainability and renewability, research focuses have shifted towards the implementation of catalytic alternatives that allow the use of *greener* oxidants, such as molecular oxygen and hydrogen peroxide[33]. Homogeneous and heterogeneous catalytic systems have been both investigated in the selective oxidative cleavage of various olefins, where *i)* homogeneous catalysts are often of difficult preparation and recoverability, and *ii)* heterogeneous catalysts are often non-selective and prone to deactivation. Nonetheless, major improvements in both fields of catalysis have been reported in literature, as well as metal-free conversions of alkenes, which are throughly discussed in the recent and excellent review by Urgoitia *et al*.[34]. Among the metal-based catalytic systems, iron catalysts show promising results in the oxidative cleavage of olefins.

In fact, as one of the most abundant, inexpensive and environmentally friendly metals on earth, iron has attracted the attention of researchers as a candidate in the synthesis of catalytic materials, finding applicability in a variety of emerging fields, ranging from energy storage to biomedicine[35,36]. Moreover, iron-based catalysis has showed potential in the *green* and selective oxidative cleavage of alkenyl aromatics (*e.g.* styrene), both in homogeneous and heterogeneous systems. As homogeneous catalysis concerns, Pillai *et al.* have reported the innovative solventless oxidation of a variety of cyclic olefins employing hydrated iron(III) nitrate and 3.4 bar of molecular oxygen at 60-80 °C, obtaining high yields in the oxidation of styrene to benzaldehyde, while lower conversion to the corresponding carbonyls were obtained for the other alkenes present in the study[37]. A ligand bearing homogeneous Fe(III)-based catalyst was instead investigated more recently by Xiao and coworkers in the aerobic cleavage of a plethora of mono- and disubstituted styrenes, showing remarkable isolated yields of the corresponding aldehydes or ketones with only 1 bar of O_2 at 70-78 °C[38].

Although homogeneous catalysis often results in exceptionally high conversions and selectivities, the reusability and separation from the reactor mixture of the catalyst still cause major concerns in the scientific community. Thus, the development of catalytic systems with facile recoverability

View Article Online
DOI: 10.1039/C7GC01405H

often resorts to heterogenization of the active material. Along these lines, the high stability and the magnetic properties of iron oxides nanoparticles make these materials attractive to use as catalytic materials[39,40]. Iron oxide is found as different polyforms including magnetite, *i.e.* Fe_4O_3 (iron(II,III) oxide); or α-Fe_2O_3 (hematite) and γ-Fe_2O_3 (maghemite), *i.e.* iron(III) oxide phases[41]. The magnetic properties of magnetite and maghemite make these oxides highly attractive as a convenient approach for separation and reusability of these materials. Furthermore, iron oxide has been proven as an effective catalyst for various oxidation reactions, *e.g.*[42-44]. In the light of these properties, iron oxide-based catalytic systems have been investigated as well in the selective oxidation of vinyl aromatics. For instance, Rak *et al.* compared hollow, etched and solid ferrite nanoshells in the conversion of styrene to benzaldehyde under 4 bar of oxygen at 90 °C, obtaining satisfactory results[45]. Hong *et al.* reported the oxidation of styrene employing iron oxide coated platinum nanowires finding acetonitrile as the best solvent and, even though the highest benzaldehyde yield was obtained with the use of molecular oxygen (38.2% at 70 °C for 24 h under 1 atm of oxygen), the highest selectivity to the aldehyde was achieved by employing hydrogen peroxide as an oxidant[46].

Since the only theoretical by-product produced is water, hydrogen peroxide has also attracted the attention of *green* researchers involved in the selective oxidation of alkenyl aromatics with remarkable results and Fe-based catalysts have been found able to activate such oxidant[47-49]. As for iron oxide concerns, Shi *et al.* investigated nano-γ-Fe_2O_3 in the oxidation of alcohols and olefins including styrene, obtaining higher yields using higher equivalents of hydrogen peroxide[50]. Exceptionally high isolated yields were reported by Rajabi *et al.* in the hydrogen peroxide-iron oxide nanoparticles oxidation of styrene derivatives in aqueous media under reflux conditions[51]. Thus, iron oxide nanoparticles coupled to hydrogen peroxide have proved to be active in the selective oxidation of alkenyl aromatics.

Vanillin is one of the most important flavouring employed in pharmaceutical, food, beverages, and perfume industries[52]; however, natural extraction of vanillin from vanilla beans only yields to a mere fraction (*ca.* 50 tons) of the total annual vanillin demand (>15000 tons), making synthetic vanillin a must[53,54]. Current production of synthetic vanillin is mainly based on the guacaiol-based route using depleting fossil feedstocks as carbon source, thus raising an environmental and sustainability concern[55], while bioconversion strategies of isoeugenol are often complex processes that lead to low vanillin yields[56-58]. Hence, more sustainable, efficient and *green* routes need to be developed, comprising the use of bio-derived substrates (*e.g.* isoeugenol) and green oxidants (*e.g.* H_2O_2).

View Article Online
DOI: 10.1039/C7GC01405H

Isoeugenol is an alkenyl aromatic present in certain essential oils, such as clove oil, tobacco, dill seed, gardenia, petunia, to name a few[59-61]; moreover, isoeugenol can be also derived from the extraction of sawdust and the controlled depolymerization of lignin, *i.e.* an important component of inedible biomass whose conversion to high-end products still requires further research[62]. For this reason, isoeugenol has been generally viewed as a model compound, facilitating the identification of the best catalyst to be further upgraded for the conversion of lignin residues. As a consequence, the selective oxidative cleavage of the vinyl group of isoeugenol is a promising strategy towards a lignin-based production of synthetic vanillin, thanks to its possible derivation from inexpensive, natural, and inedible sources. Focusing on non-enzymatic isoeugenol conversion strategies, Herrmann *et al.* investigated the use of methyltrioxorhenium catalyst in the oxidative cleavage of isoeugenol and *trans*-ferulic acid to vanillin in the presence of anhydrous hydrogen peroxide which was postulated to run *via* subsequent epoxidation and diolization steps followed by a final oxidation to vanillin[63]. Shul'pin *et al.* reported the oxidation of isoeugenol to vanillin by hydrogen peroxide with a combinative *n*-Bu_4NVO_3/pyrazine-r-carboxylic acid (PCA) catalytic system under air proposing a radical mechanism[64]. The mechanistic differences given by a strict dependency between oxidant/catalytic stystem further complicate the understanding and implementation of the oxidative cleavage of isoeugenol. Moreover, these homogeneous systems present the usual drawbacks of these types of catalysis (*vide supra*), thus incentivating research towards the use of heterogeneous catalysts. Heterogenized co-porphyrin complexes intercalated into lithium taeniolite clay were studied by Adilina *et al.*, finding a vanillin yield of 72% when employing low isoeugenol concentrations (0.3 mmol) and high 100% O_2 pressure (3 bar) in acetonitrile[65]. Benefits of a low isoeugenol concentration were also observed by Bohre *et al.* in the aerobic oxidation of isoeugenol over reduced graphene oxide-supported copper oxide, but also a higher pressure and temperature (4 bar O_2 at 50 °C) were found to suppress by-products formation and improve overall vanillin yields. Moreover, the authors suggest a synergistic effect of the electron-rich graphene oxide in stabilizing the copper species, which could be expected from the humin by-products as well[16]. Both of the aforementioned heterogeneous isoeugenol conversion studies imply the formation of a dioxygenated intermediate between the isoeugenol radical and the activated metal centre prior the selective cleavage to vanillin, discarding the epoxidation route proposed by Herrmann *et al.* (*vide supra*). A radical-free mechanism is more likely to favor the selectivity towards one particular product (*e.g.* aldehyde, epoxide), and suppress the formation of high molecular weight co-products. Thus, although an unequivocal mechanism for the selective oxidation of the vinyl group of isoeugenol has yet to be established, the consistency in the mechanistic speculations further support the investigation of heterogeneous catalytic systems. To the best of our knowledge, iron-based

View Article Online
DOI: 10.1039/C7GC01405H

heterogeneous catalysts have yet to be reported in the oxidative cleavage of isoeugenol to vanillin, in particular, if combined to a carbon-based side-product such as humins.

One of the 12 principles of Green Chemistry developed by Anastas and Warner[66] states the importance of minimizing the use of solvents whenever possible. Keeping this principle in mind, this work aimed to prove the possibility of synthesizing catalytic active materials from humins and iron precursors without the aid of any solvent. In particular, mechanochemical synthesis has taken hold as a promising route for the preparation of catalytic materials in solvent-free conditions. It was speculated that the combination of the accumulated potential energy, shear and friction forces in the milling process create a highly defective surface which could lead to an improved reactivity of the material[67]. Thus, ball milling (BM) as well as *alternative* thermal degradation (TD) techniques in the absence of any solvent were investigated for the preparation of magnetic catalytic materials, employing thermally treated (humins foams[68]) and fructose-derived humins provided by Avantium B.V. (Netherlands), respectively. The catalytic activity of these materials was subsequently investigated in the microwave-assisted selective oxidation of isoeugenol to the high added value product, vanillin.

Experimental

Materials

Humins and humins foams[69] were provided by Avantium B.V. (Netherlands) and used as received. The catalysts precursors, ferrous chloride tetrahydrate (99%, $FeCl_2 \cdot 4H_2O$) and ferric nitrate nonahydrate (≥98%, $FeNO_3 \cdot 9H_2O$) were purchased from Sigma Aldrich, as well as Fe_2O_3 and Fe_3O_4 nanopowders (nano-Fe_2O_3 and nano-Fe_3O_4, respectively) which were used as a comparison to the synthesised nanocomposites in the catalytic testing. Concerning the materials for the reaction mixture, hydrogen peroxide (50wt%) and isoeugenol (98%) were purchased from Sigma Aldrich, whereas acetonitrile (99.9%) was purchased from Panreac. All of the materials were used without further purification.

Catalyst preparation

Ferrous chloride tetrahydrate ($FeCl_2 \cdot 4H_2O$) and ferric nitrate nonahydrate ($FeNO_3 \cdot 9H_2O$) were used for the synthesis of iron oxide composites. F-BM-CL and F-BM-NO catalysts were both

View Article Online
DOI: 10.1039/C7GC01405H

prepared from humins foams (**F**) in a planetary ball mill (**BM**) Retsch, model PM 100. In particular, 2 g of ferrous chloride (**CL**) were employed for F-BM-CL, and the same amount in weight of ferric nitrate (**NO**) for F-BM-NO; the iron precursors were respectively milled at 350 rpm for 45 minutes (2 minutes intervals) with 4 g of humins foams, in order to assure the complete grinding of the carbonaceous material. Samples were subsequently dried overnight at 100 °C and calcined at 400 °C for 4 hours (β=5 °C/min).

H-catalyst series were instead synthesised by alternative thermal degradation (**TD**) of humins (**H**) and $FeNO_3 \cdot 9H_2O$. The intrinsic stickiness of humins (*caramel-like*, *i.e.* highly viscous black liquid) makes these compounds difficult to handle, therefore an uncertainty of ±0.3 g in the quantities of humins used should be taken into consideration. H-TD-C and H-TD-W were synthesised by liquefying the humins in an oven at 100 °C over the iron precursor. In particular, H-TD-C was prepared by close contact (**C**) melting of humins (4 g) over a layer of ferric nitrate (4 g) in a crucible for ten minutes at 100 °C; for H-TD-W, instead, the humins (5 g) were liquefied at 100°C from a higher altitude compared to the layer of the iron precursor (2.5 g), by employing a watchglass (**W**) over the crucible. For both samples, an increase of the volume of the solid solution has been observed, seemingly due to an incorporation of gases in the mix. A plausible explanation would be that upon decomposition of the iron(III) precursor, the humins undergo partial mineralization to CO_2, causing the visible increase of volume. Both of the samples were then manually ground, and calcined with the same conditions of the iron-foams materials (*vide supra*). For the H-TD-L and H-TD-E catalysts, discs of humins were prepared by melting the *caramel-like* carbon material at 100 °C over a non-sticky surface and subsequently solidified in a fridge. In particular, a layer (**L**) of 3 g of humins was covered with 0.66 g of iron precursor (maximum quantity that the surface of the layer could uptake) and calcined in a folded position, yielding to H-TD-L; H-TD-E was synthesised by rolling a 2 g humins disc around 1 g of $FeNO_3 \cdot 9H_2O$, in a way that all the iron(III) nitrate would be embraced (**E**) by the carbon material. Both samples were then directly calcined at 400 °C, as all the other samples.

View Article Online
DOI: 10.1039/C7GC01405H

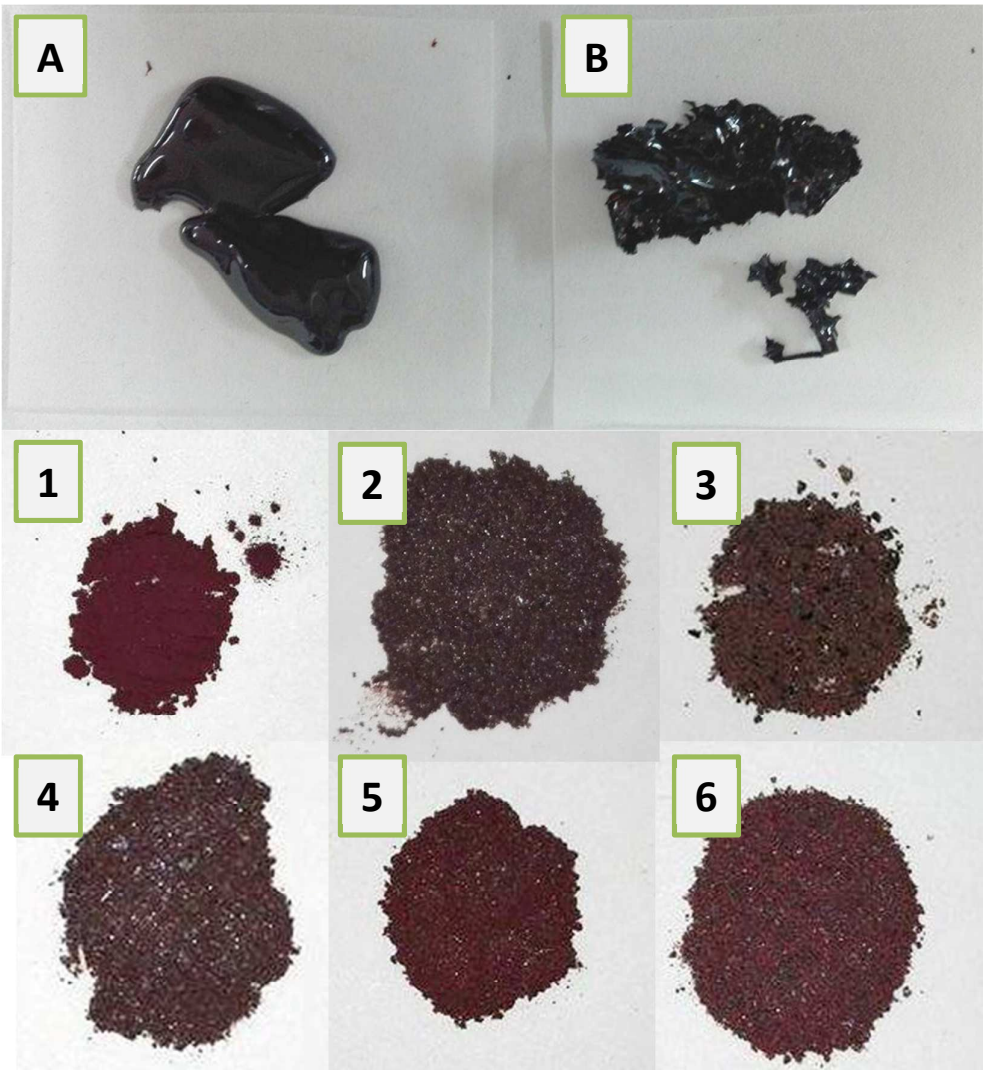

Figure 1. Images of the starting materials (A-humins, B-humins foams), and synthesised nanocomposites (1-F-BM-CL, 2-F-BM-NO, 3-H-TD-E, 4-H-TD-L, 5-H-TD-W, 6-H-TD-C).

Catalyst Characterization

Nitrogen physisorption measurements were performed at 77 K by using an ASAP 2000 volumetric adsorption analyzer from Micrometrics. Samples were degassed for 24 h at 130 °C under constant vacuum ($p<10^{-2}$ Pa) before performing the measurements. Surface areas were calculated according to the BET equation, whereas average pore diameter and pore volume were obtained from the N_2 desorption branch.

X-ray Powder Diffraction (XRD) experiments were recorder on a Bruker D8 Discover diffractometer (40 kV, 40 mA), equipped with a goniometer Bragg Brentano θ/θ of high precision,

View Article Online
DOI: 10.1039/C7GC01405H

using $Cu_{K\alpha}$ (λ=0.15406 nm) radiation. Scans were performed over a 2θ range from 10 to 80, at step size of 0.05° with a counting time per step of 143.3 s.

The chemical composition of the surface and the study of the chemical state of the elements constituent of solids were carried out by XPS. A Physical Electronics spectrometer (PHI Versa Probe II Scanning XPS Microprobe) was used, with scanning monochromatic X-ray Al Kα radiation (100 μm, 100 W, 20 kV, 1,486.6 eV) as the excitation source, and a dual beam charge neutralizer. High-resolution spectra were recorded at a given take-off angle of 45° by a concentric hemispherical analyzer operating in the constant pass energy mode at 23.5 eV, using a 1400 μm line (with a 100 μm diameter of the x-ray highly focused beam) analysis area. The spectrometer energy scale was calibrated using Cu $2p_{3/2}$, Ag $3d_{5/2}$, and Au $4f_{7/2}$ photoelectron lines at 932.7, 368.2 and 84,0 eV, respectively. Under a constant pass energy mode at 23.5 eV condition, the Au $4f_{7/2}$ line was recorded with 0.73 eV FWHM at a binding energy (BE) of 84.0 eV. PHI Smart Soft-VP 2.6.3.4 software package was used for acquisition and data analysis. A Shirley-type background was subtracted from the signals. Recorded spectra were always fitted using Gauss–Lorentz curves. Atomic concentration percentages of the characteristic elements of the surfaces were determined taking into account the corresponding area sensitivity factor for the different measured spectral regions.

Scanning electron micrographs (SEM) and elemental composition of materials were recorder using both the JEOL JSM 6300 and the JEOL JSM 7800F microscopes, the latter employed for energy-dispersive X-ray microanalysis (EDX) X-max 250 (detector SiLi, ATW2), at 20 kV.

Transmission electron micrographs (TEM) were recorded on a JEOL JEM 1400 instrument at 120 kv with a lattice resolution of *ca.* 0.4 nm. Samples were suspended in ethanol and deposited straight away on a copper grid prior to analysis.

Magnetic susceptibility was measured at room temperature with the Bartington MS-2 instrument at low frequency (470 Hz).

Catalytic testing

The microwave-assisted oxidation of isoeugenol to vanillin was performed in a CEM-Discover microwave reactor equipped with a PC-controlled interface. In particular, the Discover

View Article Online
DOI: 10.1039/C7GC01405H

method in a sealed vessel was employed, which allows the system to build up pressure with the formation of gaseous products during the reaction. The observed pressure increase could however not be ascribed to mineralization of isoeugenol to CO_2, or decomposition of H_2O_2 to O_2, based on ideal gas law calculations. In all experiments, 2.5 mg of catalyst, 0.2 mL of isoeugenol, 0.3 mL of H_2O_2 (50wt%), and 1 mL of acetonitrile were employed, under 300 W of irradiation. Different reaction times were carried out for these experiments, due to the runaway character of the oxidation (rapid increase of pressure). Therefore, 3 minutes reactions with a maximum reachable temperature of 140 °C under variable irradiation (0-300 W) were performed in order to have a better understanding of the catalytic activities. Blank reactions were also carried out under these conditions, in particular, were carried out: *i)* a reaction with solely the reagent mixture, *ii)* a reaction with the reagent mixture in the presence of the humins foams (2.5 mg), *iii)* a reaction in the presence of (commercial) nano-Fe_2O_3 and *iv)* a reaction in the presence of presence of (commercial) nano-Fe_3O_4 (2.5 mg). Recyclability tests were run for all the magnetic nanocomposites up to the first reuse with 2.5 mg of catalyst. Reusability was investigated for the most stable nanocomposites with 50 mg of catalyst, in the same reaction conditions stated before. Results were analysed by GC using an Agilent 7890A fitted with a Supelco column (100 mx0.25 nmx0.5µm) and a flame ionization detector (FID). Quantification of the products was obtained from the ratio of the corresponding peak areas, as justified by a close agreement of some representative product/reagent mixtures compared against a multicomponent calibration curve previously done by our research group. Furthermore, no solid residues or increase in viscosity was observed at the end of the reactions, thus indicating no unwanted polymerization of isoeugenol. This further was substantiated by consistent total peak areas in the GC analysis (*vide supra*). The reaction products were confirmed by HPLC and GC-MS analysis, carried out by the staff of the Central Service for Research Support (SCAI) of the University of Córdoba, Spain.

Results and Discussion

The catalysts presented in this study have been synthesised via ball milling of humins foams with two different iron precursors (F-BM-CL, iron(II) chloride; and F-BM-NO, iron(III) nitrate) or by alternative thermal degradation of humins combined to Fe(III) nitrate in alternative ways, resulting into the H-catalyst series (H-TD-E, H-TD-L, H-TD-C, H-TD-W). In particular, H-TD-E and H-TD-L were synthesised by employing humins discs either embracing (H-TD-E) or being covered (H-TD-L) by the iron precursor; H-TD-C and H-TD-W were instead prepared by the

View Article Online
DOI: 10.1039/C7GC01405H

melting of humins either in close contact with the iron precursor (H-TD-C) or from a higher altitude (H-TD-W) with the aid of a watchglass over the crucible.

The resulting textural properties determined by the BET-N_2 physisorption method of the composites are summarised in Table 1. The physical nature of humins implies no porosity, whereas the BET analysis of humins foams (entry 2) shows generally low values of surface area and pore volume. Interestingly, all of the composites, present systematically higher surface areas and pore volumes, with pore diameters in the mesopore range (2-50 nm). Prominently, the use of the ferrous chloride precursor (F-BM-CL, entry 3) led to a very low surface area solid (*ca.* 8 m^2/g), found to be consistently higher when ferric nitrate was employed ($S.A._{F\text{-}BM\text{-}NO}$=34 m^2/g). For the H-series, H-TD-L possessed the highest surface area with a smaller average pore diameter, given probably by the layer disposition of the iron(III) precursor on the humins disc; the encapsulation of iron(III) nitrate into a humins disc (H-TD-E, entry 5) led, as expected, to a lower surface area and pore volume. Nonetheless, the average pore diameter of the H-TD-E composite is larger as compared to other H-series materials, signalling the formation of shorter and wider pores, probably due to the spatial constriction given by the humins embrace during preparation.

Table 1. Textural properties of humins and foams composites.

		Surface area/ $m^2\ g^{-1}$	Pore volume/ $cm^3\ g^{-1}$	Average pore diameter/ Nm
1	Humins[a]	-	-	-
2	Foams[b]	<5	0.06	11.8
3	F-BM-CL	<10	0.11	43.2
4	F-BM-NO	34	0.15	12.5
5	H-TD-E	20	0.11	16.4
6	H-TD-L	58	0.19	9.6
7	H-TD-W	45	0.20	12.9
8	H-TD-C	43	0.17	12.1

View Article Online
DOI: 10.1039/C7GC01405H

[a]Physical nature of humins (black liquid phase) does not allow BET analysis

[b]Starting material of F-catalyst series

Powder X-ray Diffraction (XRD) analysis results of the materials are presented in Figure 2. The high intensity of the peaks show a high degree of cristallinity for all the samples. In particular, F-BM-CL presents an almost pure hematite phase, indicating the previously reported oxidation of Fe(II) precursor to Fe(III) during the preparation under ambient atmosphere[49,69]. Mixtures of iron oxide phases were observed, with a lower degree of cristallinity, when Fe(III) precursors were employed probably due to impurities. In fact, the peak at 33.1° (*, Figure 2) is typical of hematite, whereas the 2θ=35.5 (°, Figure 2) can be adscribed to either maghemite, magnetite, or hematite, indistinguishable by XRD. As a first analysis, F-BM-NO and H-TD-L exhibited a higher hematite content (H-TD-C has an almost 50:50 ratio of the iron oxides phases), while H-TD-W and H-TD-E have a lower hematite content. XRD analysis of H-TD-E also shows the presence at 31.6° and 33.7° (#, Figure 2), probably due to the presence of impurities including sodium sulfate or similar most probably coming from the humins matrix.

View Article Online
DOI: 10.1039/C7GC01405H

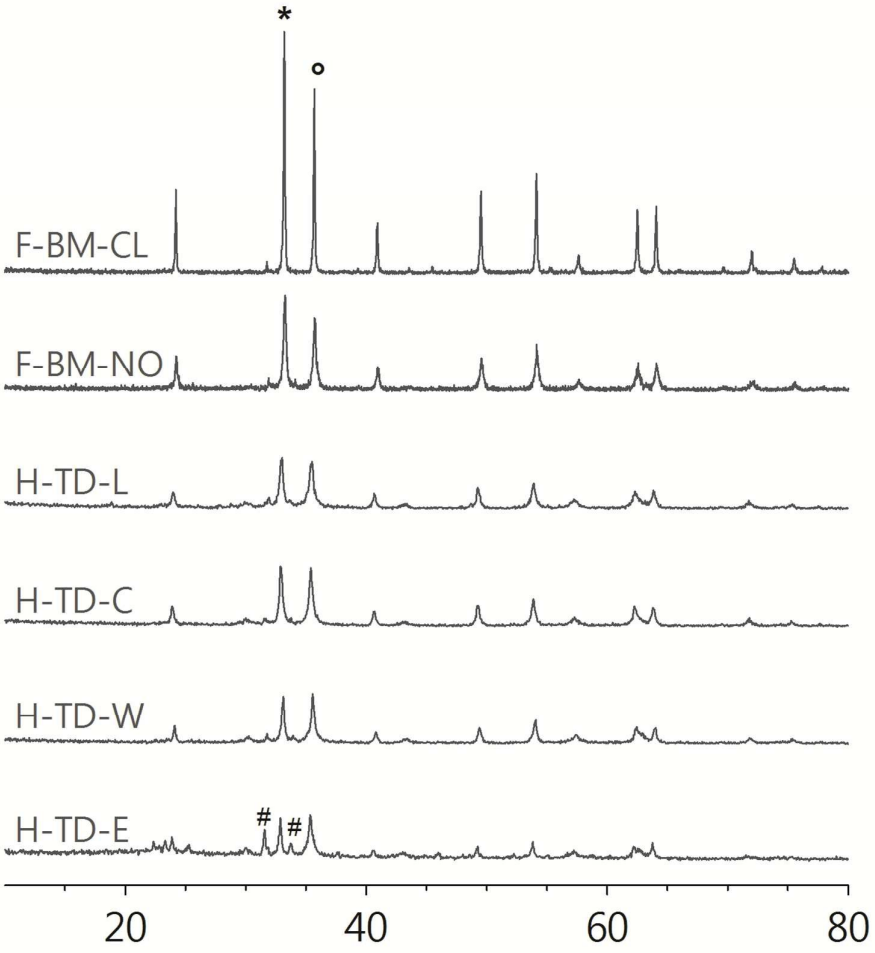

Figure 2. XRD patterns of the F- and H-series composites. (*,hematite; °, either maghemite, magnetite, or hematite; #, sodium sulfate or similar, *see text*)

In fact, X-ray Photoelectron Spectroscopy (XPS) analysis showed for all the samples the presence of Fe, C and O (Table 2), but also Cl (0.3-1.1 wt%), S (1.1-7.6 wt%, as sulfate) and Na (3.5-13.3 wt%), in good agreement with XRD results and supporting its procedence from intrinsic impurities in humins and foams. In particular, H-TD-E showed the highest sodium and sulfur contents of respectively 13.3 wt% and 7.6 wt%, which justifies the presence of the unidentified XRD peaks (*vide supra*). Importantly, only Fe(III) species were found for all the samples (Figure 3), concluding that the composites are mixtures of hematite and maghemite phases, except for F-BM-CL which is purely hematite (see XRD).

View Article Online
DOI: 10.1039/C7GC01405H

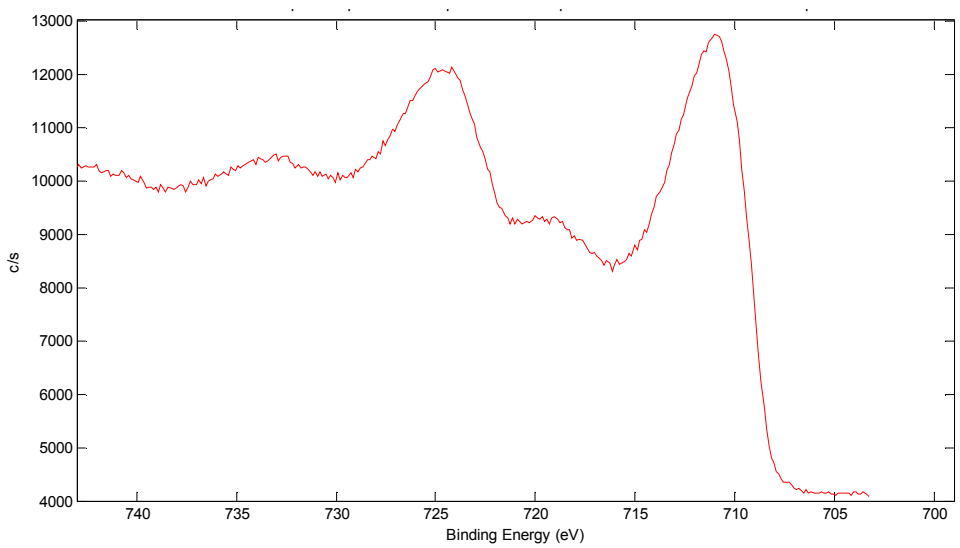

Figure 3. XPS spectra of the Fe2p regions of F-BM-NO, representative of all the nanocomposites.

Detailed analysis of the C 1s spectra (Figure 3) showed the presence of C-C (48.7-70.2%), C-O (19.3-34%), C=O (3.8-12.4%), and $–COO^-$ (4.8-8.6%) species. These contributions can be adscribed to residual humins which are expected to have a higher degree of aromatization upon heating as previously found by Hoang[9] and van Zandvoort[14], which might lead to rapid electron trasmission, thus higher catalytic activity.

Table 2 summarises the mass concentrations of Fe, C, and O obtained from XPS, alongside the magnetic susceptibility of the composites. The use of Fe(II) chloride precursor led to a non-magnetic material (F-BM-CL, entry 1), whereas the use of Fe(III) nitrate resulted in the formation of promising magnetic nanocomposites.

Table 2. Mass concentrations of iron, carbon and oxygen deducted by XPS analysis, and magnetic susceptibility.

		Mass Concentrations (%)			Magnetic susceptibility/
		Fe2p	C1s	O1s	10^{-6} m^3 kg^{-1}
1	F-BM-CL	46.28	11.07	34.99	-[a]
2	F-BM-NO	53.85	9.27	33.63	51.8
3	H-TD-E	39.64	15.07	36.25	118.9

View Article Online
DOI: 10.1039/C7GC01405H

4	H-TD-L	48.72	9.08	35.12	176.8
5	H-TD-W	57.12	6.28	32.14	202.3
6	H-TD-C	57.06	8.11	31.9	178.4

[a]Non-magnetic material

For the H-series catalysts, it is possible to correlate a higher iron concentration to a greater magnetic susceptibility, thus a lower hematite content, in line with the first interpretation by XRD analysis. Nonetheless, the extremely high superficial oxygen content (>50 at.%, XPS) suggests a potential use of these composites as oxidation catalysts. The order of iron content determined by XPS decreased in the order: H-TD-W≈H-TD-C>F-BM-NO>H-TD-L>F-BM-CL>H-TD-E.

Morphology studies and SEM-EDX of the foams and humins composites show a highly defective and non-homogeneous surface for most of the samples. Tendentiously, the composites form curious agglomerates from which independet nanoparticles can be clearly visualised at higher magnifications.

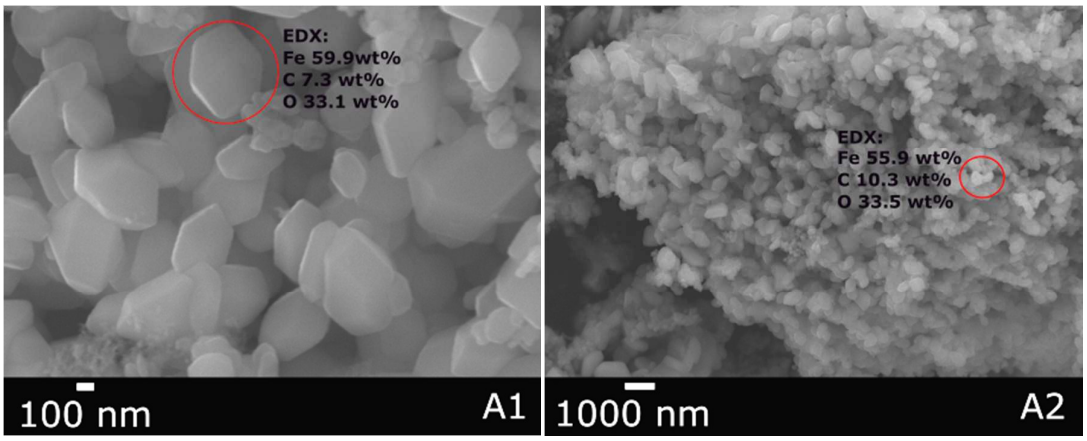

View Article Online
DOI: 10.1039/C7GC01405H

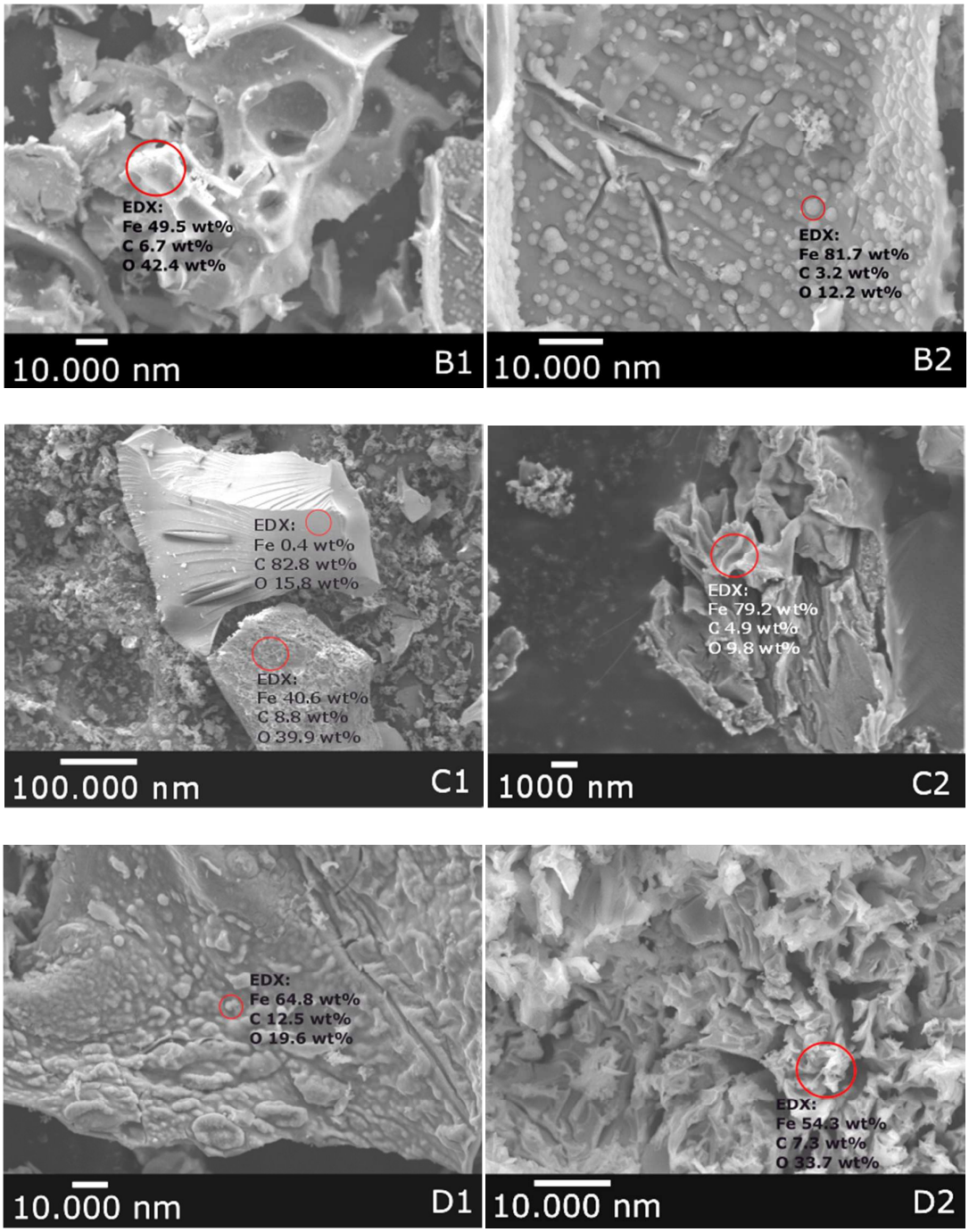

View Article Online
DOI: 10.1039/C7GC01405H

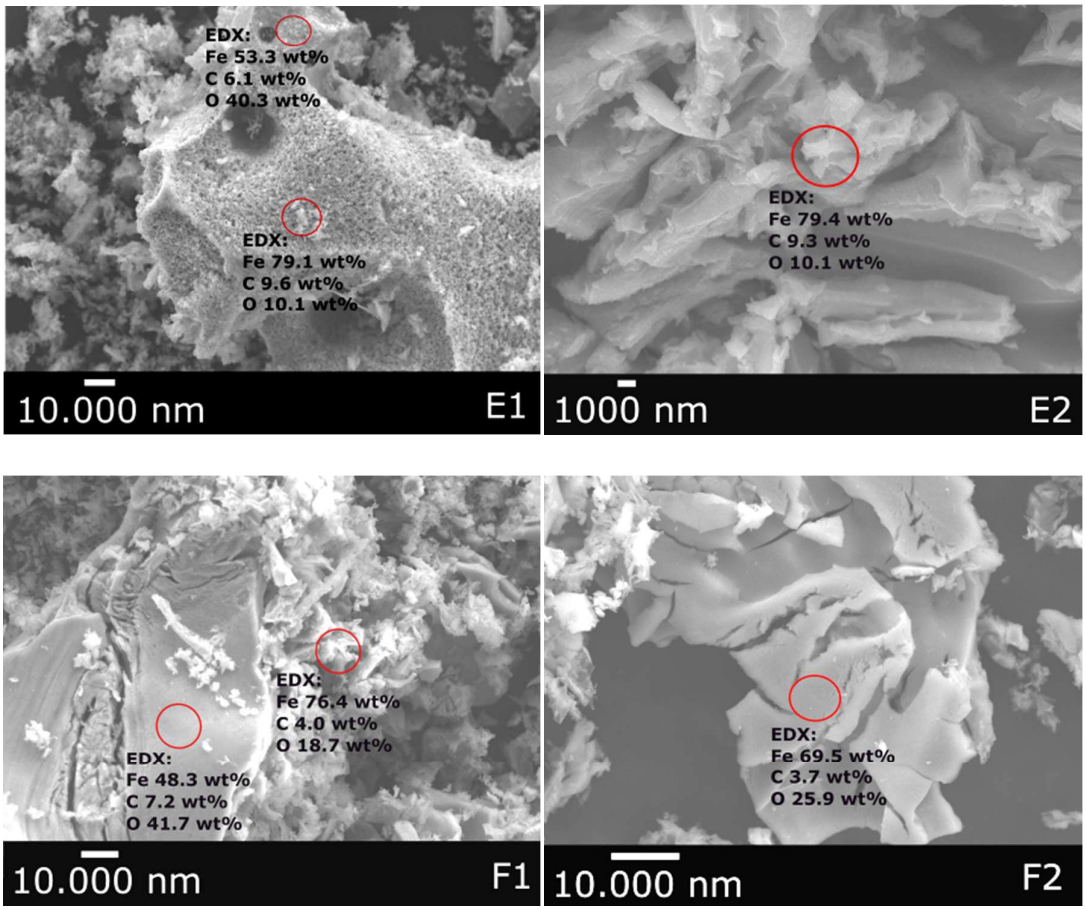

Figure 4. SEM micrographs of the iron oxide/humins composites. A1-A2: F-BM-CL; B1-B2: F-BM-NO; C1-C2: H-TD-E; D1-D2: H-TD-L; E1-E2: H-TD-W; F1-F2: H-TD-C.

SEM micrographs of F-BM-CL (Figure 4-A) shows the most regularity in shape, being hexagonal particles of various sizes (100-500 nm), in good agreement with the crystal lattice shape of iron oxide nanoparticles from TEM analysis (Figure 5-A). The hexagonal particles of F-BM-CL were found to contain *ca.* 56wt% Fe, 10wt% C and 33 wt% O, and the remaining 1wt% as impurities (*i.e.* Na, S, and Cl) *via* SEM-EDX analysis independent from the area of sampling, showing a fairly homogeneous sample. Similar values of weight percentages of the elements found with XPS analysis (*vide supra*) suggests the presence of iron oxide both in the bulk and the surface of the particles. The strucuture of F-BM-NO (Figure 4-B1), instead, reminds the macroscopic structure of untreated humins foams (Figure 1-B), however presenting embedded spherical iron-rich particles (SEM-EDX: Fe 82wt%, C 3wt%, O 12wt%) of the order of 1-2 μm (Figure 4-B2). This could be given by the reduction by carbon of the iron(III) species towards metallic iron, creating an iron-rich core. TEM analysis of F-BM-NO (Figure 5-B) depicts irregular nanoparticles of 20 nm on

View Article Online
DOI: 10.1039/C7GC01405H

average (extremes identified as between 6 and 32 nm) arranged to create a porous material, suggesting that the ball milling of foams and iron(III) nitrate gave a simil-template synthesis.

The H-series of materials are even less homogeneous, even at higher magnification. SEM micrographs show a more flake-like structure of iron oxide agglomerates in all samples, however differing from the preparation method (Figures 4-C,-D,-E,-F). For instance, H-TD-L, where the iron precursor was layered on a humins disc, shows areas where the iron oxide has directly deposited onto the disc (Figure 4-D1, SEM-EDX: Fe 65wt%, C 13wt%, O 20wt%), with the flake-like structures having an elemental composition of similar order (Figure 4-D2, SEM-EDX: Fe 54wt%, C 7wt%, O 34wt%). On the other hand, for the carbon-embraced iron precursor preparation which resulted in H-TD-E, SEM-EDX analysis shows blocks of high carbon content materials (Figure 4-C1, SEM-EDX: Fe 0.4 wt%, C 83wt%, O 16wt%), probably derived from the outside shell of the humins disc not in contact with the iron precursor, and at the same time flake-like structures of high iron content (Figure 4-C2, SEM-EDX: Fe 79wt%, C 5wt%, O 10wt%). Figure 3-E and –F show instead the SEM pictograms of the samples prepared by either close contact or higher altitude melting of humins, thus H-TD-C and H-TD-W, respectively. SEM-EDX of both samples showed high iron content of the flake-like structures in a similar fashion as H-TD-E, finding 76wt% of iron for H-TD-C (Figure 4-F1) and 79 wt% for H-TD-W (Figure 4-E2). As for F-BM-NO (*vide supra*), the presence of humins could reduce the iron species towards a zero-valent state. Figure 4-F2, instead, shows a highly defective iron oxide block in H-TD-C (SEM-EDX: Fe 69wt%, C 4wt%, O 26wt%) which resembles a carbonaceous agglomerate, suggesting again a template-like synthesis.

TEM images (Figure 4-C, -D, -E, -F) of the H-series show, where possible to determine, nanoparticles of up to 300 nm, with the majority in the 4-30 nm range. In general, an amorphous carbon can be identified in the samples, often making it difficult to determine the single nanoparticles. Figures 5-C1, -D1, -F1, and -F2 are representative of the challenging determination of the nanoparticles in the various samples, almost resembling high resolution pictograms of solid solutions. Figure 5-C2, in particular, shows what resembles a carbon block decorated with nanoparticles in the range of 12-14 nm. This could be ascribed to the chosen synthesis of this sample (*i.e.* H-TD-E), since the encapsulation of the iron precursor by the humins layer might have dispersed the nanoparticles in the carbon matrix.

View Article Online
DOI: 10.1039/C7GC01405H

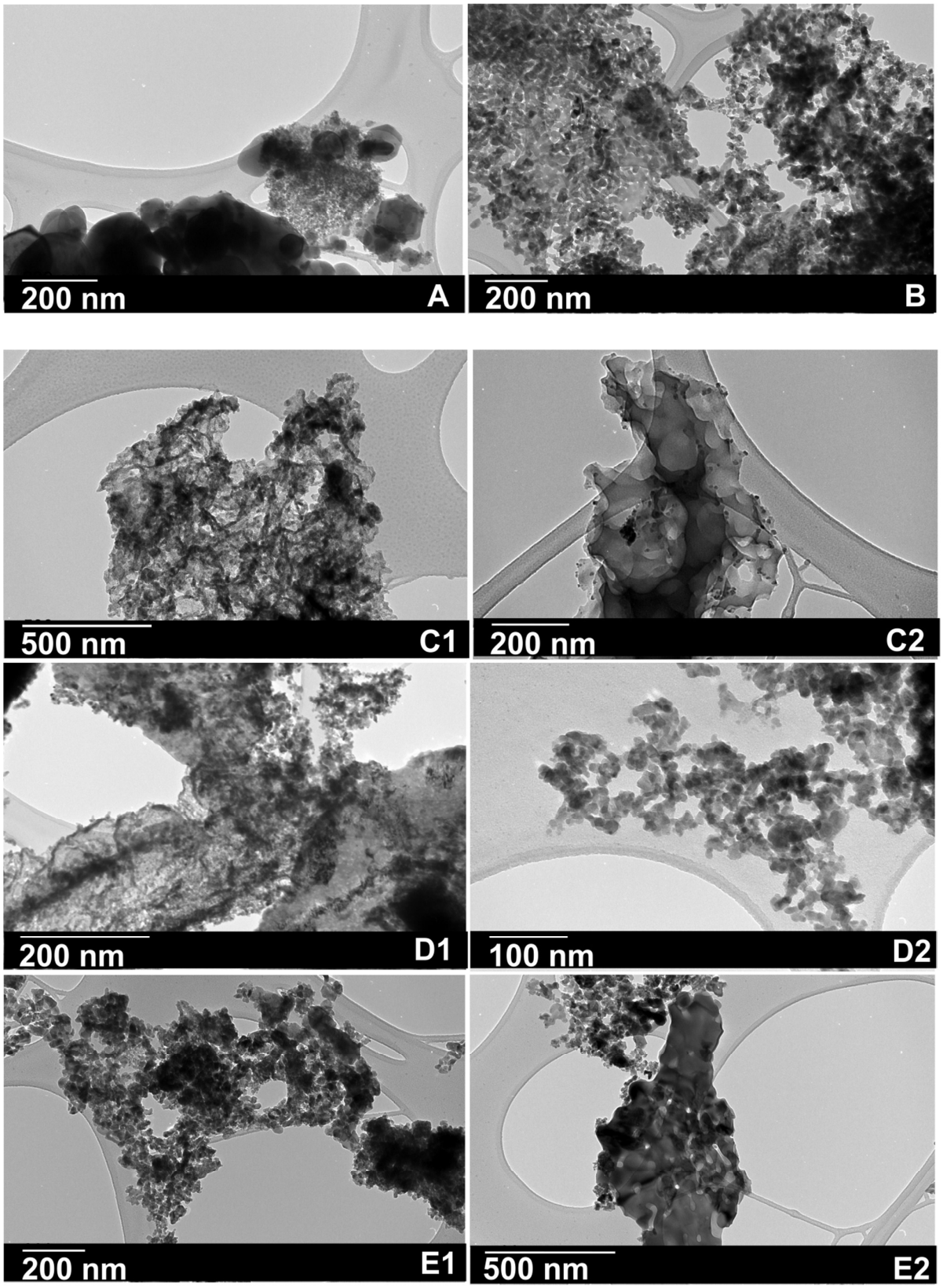

View Article Online
DOI: 10.1039/C7GC01405H

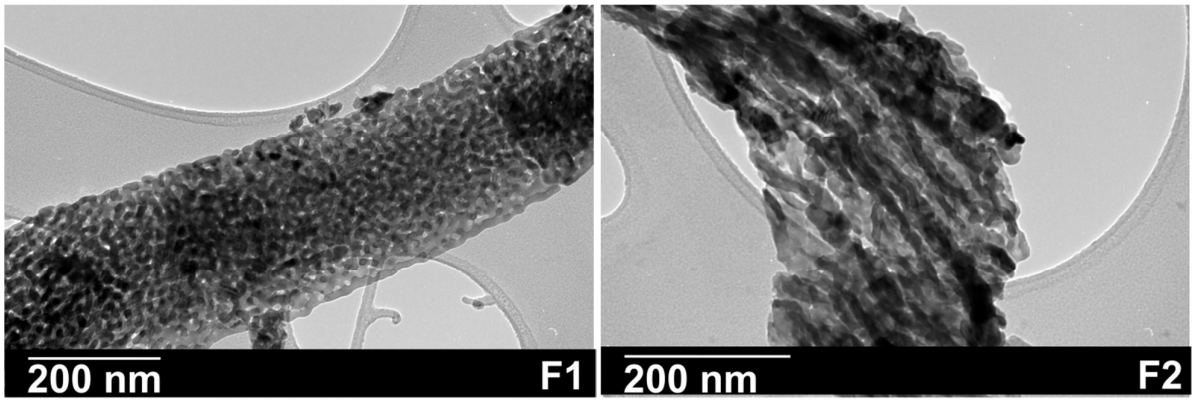

Figure 5. TEM micrographs of the iron oxide/humins composites. A: F-BM-CL; B: F-BM-NO; C1-C2: H-TD-E; D1-D2: H-TD-L; E1-E2: H-TD-W; F1-F2: H-TD-C.

Catalytic activity of all synthesized nanocomposites was subsequently investigated in the microwave-assisted selective oxidation of isoeugenol to vanillin (Scheme 2) at a fixed microwave power (300 W) with a remarkably low catalyst loading of 2.5 mg. Results of conversion and selectivity for the different catalytic systems have been summarised in Table 3, obtaining the optimum results for F-BM-CL with selectivity over 60% to vanillin at *ca.* 90% conversion after 2 minutes reaction. In general, high conversions could be achieved (>87%), with selectivities to vanillin ranging between 42 and 64%, although with each system requiring different reaction times and reaching different temperatures, though of similar order.

Table 3. Catalytic activities of the humins/foams composites in the microwave-assisted oxidation of isoeugenol to vanillin.

	Catalyst	Time (min)	T (°C)	P (PSI)	Conversion (%)	Selectivity (%)
1	F-BM-CL	2.2	169	241	89	64
2	F-BM-NO	4.8	152	246	88	54
3	H-TD-C	4.2	152	246	89	63
4	H-TD-W	3.5	155	244	91	63
5	H-TD-E	5.5	156	247	>99	50

View Article Online
DOI: 10.1039/C7GC01405H

6	H-TD-L	4.7	149	248	>99	42

Reaction conditions: 2.5 mg of catalyst, 0.2 mL isoeugenol, 0.3 mL H_2O_2 (50wt%), 1 mL acetonitrile, irradiation of 300 W until runaway reaction.

Conversion of isoeugenol with hydrogen peroxide by the humins-iron oxide nanocomposites leads to vanillin as main reaction product, alongside a plethora of by-products (Scheme 2), comprising vanillin methyl ketone (**1**), isoeugenol diol (**2**), eugenol (**3**), and dihydrodiisoeugenol (**4**), with **1** and **2** being the most prominent co-products, in order. Similar molecules were reported in the past reports of said reactions[16,63-65]. In particular, the literature on the conversion of isoeugenol to vanillin claimed maximum: *a*) 50% yield at 80 °C and 0.4 M of H_2O_2 after 2 hours[64]; *b*) 53% yield at 50 °C and 4 bar of O_2 after 24 hours[16]; and *c*) 72% yield at 50 °C and 3 bar of O_2 after 24 hours[65]; the nanocomposites reported herein, instead, grant vanillin yields between 42-57% in less than 5 minutes of reactions, although at higher operating temperatures (*i.e.* 149-169 °C). Nonetheless, further optimization of the reaction conditions is needed, as well as a better understanding of the mechanism of reaction.

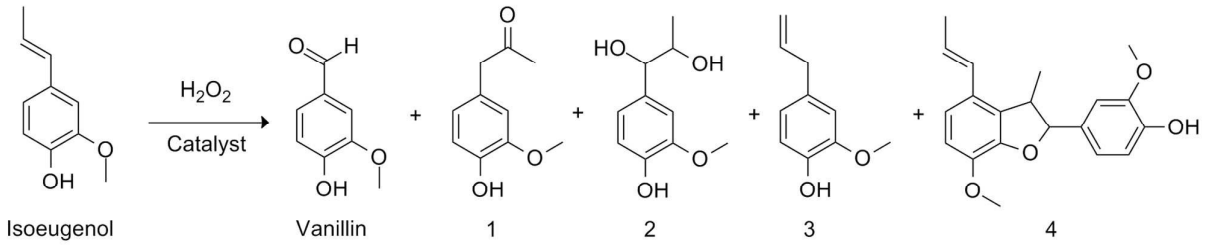

Scheme 2. Reaction scheme of isoeugeneol conversion to vanillin and co-products: vanillin methyl ketone (**1**), isoeugenol diol (**2**), eugenol (**3**), and dihydrodiisoeugenol (**4**), presented in order of magnitude.

By analyzing the reaction products, a mechanistic evaluation might be drafted. Notably, the absence of vanillic acid as co-product with our strong oxidizing conditions (isoeugenol/H_2O_2 ratio: 1:5) and high temperature is rather surprising. Nonetheless, this particular compound was only reported within biotransformations of isoeugenol to vanillin[70,71], suggesting that both homogeneous and heterogeneous catalytic systems do not promote further oxidation of vanillin to its carboxylic acid form. In fact, kinetic studies on vanadium complexes carried out by Shul'pin research group[64] suggested a faster consumption of isoeugenol compared to vanillin under oxidizing conditions, therefore limiting the formation of vanillic acid. Thus, short reaction times, such as the ones

View Article Online
DOI: 10.1039/C7GC01405H

reported herein, would minimize the formation of higher oxidized products, although a higher temperature is required in order to activate the catalytic material in such small time frame. Moreover, isoeugenol epoxide was not detected among the reaction products, in contrast to the aforementioned reports; this difference with literature can be simply ascribed to the water-rich environment given by the H_2O_2 aqueous solution employed which favors the hydrolysis to the observed corresponding diol (**2**), whereas the previous findings in literature operated in anhydrous environments (O_2 or anhydrous H_2O_2). Furthermore, the production of **4** suggests the formation of radical intermediates of isoeugenol which undergo radical coupling, as supported by previous reports (e.g.[16]). However, first row transition metal-catalyzed oxidations with hydrogen peroxide are believed to follow the non-radical oxometal pathway[33], where H_2O_2 oxidizes the metal centers that eventually coordinate the reagent. Furthermore, the contribution from residual humins must be taken into consideration. In fact, disordered and electron-rich carbon materials have been found to be highly active in the decomposition of hydrogen peroxide into radicals[72]. The synergy between the metal and carbon active sites further complicates the understanding of the overall mechanism governing the reaction; however, the absence of higher condensation or polymerization products may suggest the prevalence of a non-radical mechanism, which can be justified by the higher concentration of iron species on the surface (see XPS). Nonetheless, further kinetic studies are indeed required to further ascertain the mechanism of iron-carbon nanocomposites. As the scope of this work is to prove the employability of humins as carbon source for catalytic purposes, particular focus is given to the selectivity to vanillin throughout this study.

Due to the fixed microwave power employed, resulting into different reaction temperatures and time, the catalytic activity of the nanocomposites cannot be unequivocally ascribed. As an attempt to better compare the catalytic activities, all reactions were performed for 3 minutes with a maximum reachable temperature of 140 °C, with the same catalyst loading, and results are reported in Table 4. A blank test of the reaction (no catalyst) was carried out under these conditions (Table 4, entry 0), also in the solely presence of the humins foams (*i.e.* the support for the F-BM-CL and F-BM-NO nanocomposites) (Table 4, entry 1), and commercial Fe_2O_3 and Fe_3O_4 nanopowders (Table 4, entry 2 and 3, respectively).

View Article Online
DOI: 10.1039/C7GC01405H

Table 4. Catalytic activities of the humins/foams composites in the oxidation of isoeugenol to vanillin under microwave irradiation (300 W), with a maximum temperature of 140 °C.

	Catalyst	Time (min)	T (°C)	P (PSI)	Conversion (%)	Selectivity (%)
0	Blank	3	120*	67	36	<20
1	Foams	3	140	120	91	<20
2	nano-Fe_2O_3	3	140	N/A	25	<20
3	nano-Fe_3O_4	3	140	N/A	28	<20
4	F-BM-CL	3	140	96	76	48
5	F-BM-NO	3	140	103	66	26
6	H-TD-E	3	140	112	66	32
7	H-TD-L	3	140	120	75	47
8	H-TD-W	3	140	107	53	35
9	H-TD-C	3	140	95	60	28

*Temperature results lower due to the absence of a catalytic material

In general, the results evidenced a moderate to high activity of all nanocomposites under the investigated conditions, improved as compared to the blank reactions. Notably, the humins foams resulted into an incredibly remarkable conversion of >90%, although with low selectivity to vanillin. This is a clear signal that humins, similar to that reported for graphene oxide[16], possess exceptional oxidation properties thanks to the high presence of electron-rich functionalities. The low selectivity to vanillin might be ascribed to higher H_2O_2 decomposition rates into unselective radical species. However, an extreme loss of the support at the end of the reaction was observed, suggesting that the humins themselves might undergo oxidation by OH• species. When the commercial nanopowders were employed (entry 2 and 3), low conversion were obtained (<30%), even lower as compared to the blank reaction in the absence of any catalytic material (36%, entry 0). This could be ascribed to differences in the governing mechanisms, where *i)*the solely presence of hydrogen peroxide under microwave irradiation leads to the formation of OH• species and, thus, fair conversion although unselective; whereas *ii)*the commercial nanopowders promote the non-radical oxometal pathway, although resulting ineffective activity under the same reaction conditions. This strongly suggests that a positive synergistic effect must exist between the iron oxide and carbon residues, given by the systematically higher conversions and selectivities of the

View Article Online
DOI: 10.1039/C7GC01405H

nanocomposites (Table 4, entry 4-9). Surprisingly, vanillic acid was detected only when nano-Fe_3O_4 (*i.e.* Fe(II) and Fe(III) mixed oxide, *alias* magnetite) was employed. A reason for the over oxidation of vanillin to its carboxylic acid could be given by a possible higher oxidation activity of the Fe(II) species present in the magnetite nanopowder, which further limit the selectivity to vanillin. This speculation is in line with the proposed mechanism of styrene oxidation by iron(III) nitrate species[37].

As for the nanocomposites synthesized for this study, F-BM-CL (entry 4) yielded to the highest conversion and selectivity to vanillin. This result can be ascribed to the larger presence of highly crystalline hematite in the catalyst, which has been found to be the active iron oxide phase[73]. Comparably, the order of reactivity (in terms of conversion) for the maghemite-hematite mixed phase catalysts was found to be as follows: H-TD-L>H-TD-E>F-BM-NO>H-TD-C>H-TD-W.

According to the findings of Gurol and Lin[74], hydrogen peroxide activation should be directly proportional to the iron oxide concentration. However, by analyzing the conversion efficiency of the H-series catalysts (Table 4, entry 6-9), the superficial iron concentration (see XPS), and the relative hematite/maghemite concentration (see XRD), a similar trend is evidenced if considering solely the hematite concentration. This suggests that hematite is thus the catalytically active morph of iron oxide. Along these lines, the higher activity of H-TD-L could thus be attributed to the higher hematite content. From a synthetic point of view, the use of a layer (disc) of humins in the synthesis of H-TD-L and H-TD-E has led to better performing catalytic materials, as compared to the use of *native* humins (namely in the preparation of H-TD-C and H-TD-W). The process of melting and subsequent cooling the humins into a thin layer might induce the polymeric chains to re-orientate in a more crystalline conformation, playing an overall positive effect in the electron transfer ability of the by-products.

Recyclability tests were subsequently conducted for all catalysts, with those presenting magnetic properties included in Figure 6. Substantial loss of activity (-15% *ca.*) is noted for the H-TD-L and H-TD-C composites, whereas only a very small activity loss (<5%) could be observed for reused H-TD-E material. Comparably, F-BM-NO and H-TD-W fully preserved their initial activity after the first (Figure 6), illustrating their potential-particularly F-BM-NO and F-BM-CL as highly stable and reusable humin-based oxidation catalysts. We believe the stability of F-BM-CL and F-BM-NO systems relates to its mechanochemical synthesis and thus inherent chemical modification of the surface in the final material, in good agreement with previous studies of the group[49]. Additionally, no colour change was observed in the final solution/filtrate after recovery of the catalyst, which may indicate a negligible Fe leaching. In contrast, the high stability of H-TD-W

View Article Online
DOI: 10.1039/C7GC01405H

may be related to the observed phase transition from maghemite to hematite after reuses (results not shown). The final solution after reaction was also yellowish, in good agremeent with similar results observed for F-BM-NO. H-TD-W and F-BM-NO were therefore investigated further up to four reuses, with a higher catalyst loading of 50 mg in the same reaction conditions.

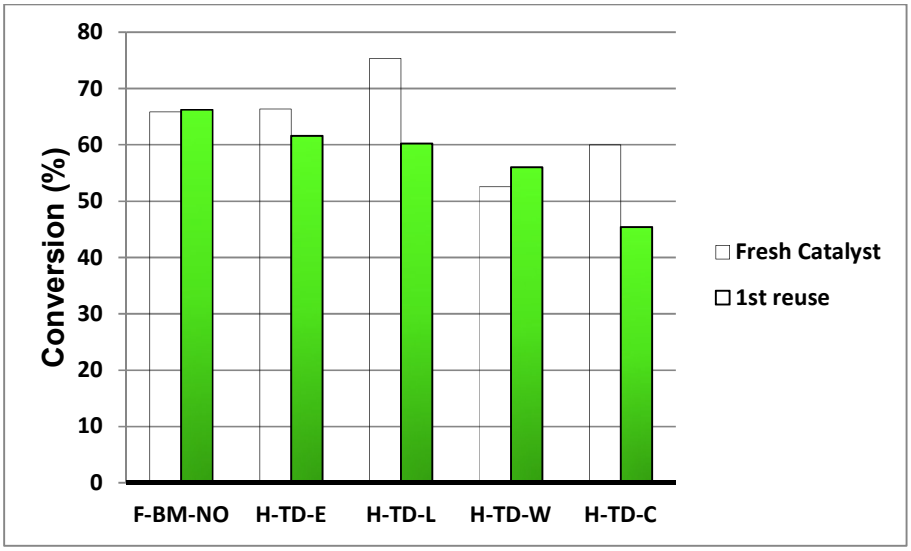

Figure 6. Recyclability tests for the magnetic humins/foams composites.

Figure 7 shows conversion and selectivity of the two nanocomposites, F-BM-NO and H-TD-W. To be noted, a higher catalyst loading (20 times higher) did improve the conversion of isoeugenol, but at the expense of the selectivity, in particular for the sample H-TD-W. This could be ascribed to a higher hydrogen peroxide decomposition rate which decreases the selectivity to the aldehyde, while favoring the formation of the co-products, in particular the vanillin methyl ketone (Scheme 3, **1**). At a first glance, an incredible stability can be seen for both of the catalysts, however a curious behaviour has been noted for the H-TD-W composite. In fact, the results of the 4th reuse of H-TD-W are referred to a spontaneous room temperature reaction (see video, ESI) that occurred when the catalyst entered in contact with the reaction medium. Fe content after reaction (filtrate/reused catalyst) measured by ICP/MS showed negligible leaching (<2ppm Fe into solution, cumulative after five use) after subsequent reuses, with investigated catalysts (*i.e.* F-BM-NO and H-TD-W) exhibiting an almost Fe content in the 4th reused catalyst as compared to the fresh one (<5% Fe loss after 5 uses).

View Article Online
DOI: 10.1039/C7GC01405H

Overall, not only a satisfactory vanillin yield is obtained, but also the nanocomposites seems to improve its activity with its use. This could be ascribed to a phase rearrangement of the nanocomposites iron oxide phase towards a more active specie, *i.e.* hematite, arising from the oxide/peroxide functionalities of the humins residue. Nonetheless, this behaviour could represent a breakthrough in both the carbon-based materials (*e.g.* humins) and the catalysis fields.

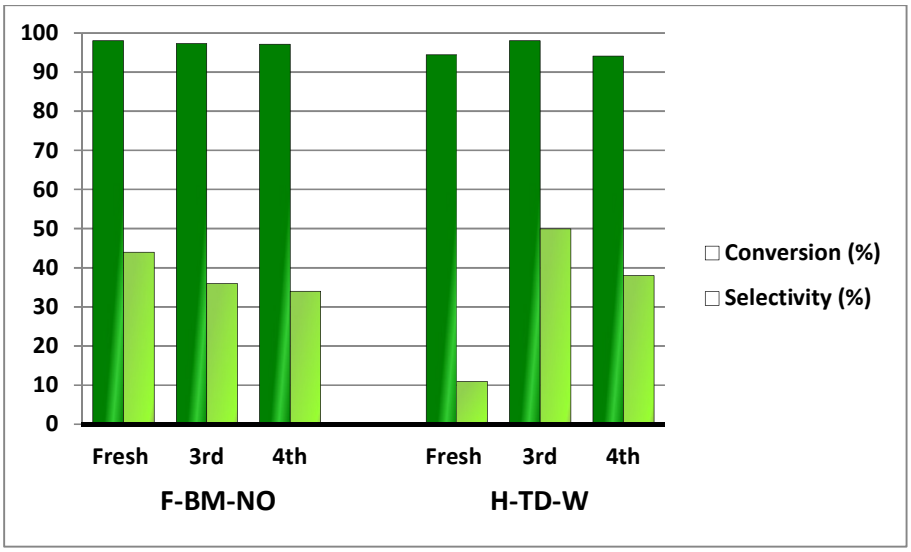

Figure 7. Recyclability runs for F-BM-NO and H-TD-W up to the fourth reuse with increased catalyst loading (50 mg).

In any case, further investigations are already ongoing to fully understand and improve the chemical structure, surface and stability of the synthesized humin/iron nanocomposites, alongside the optimization of the reaction conditions for the production of vanillin from lignocellulosic derivatives.

Conclusions

Humins have been generally regarded as undesired by-products in the acid-catalyzed conversion of biomass. This work shows the possibility of employing humins in the preparation of catalytic nanocomposites. All of the composites were prepared via solvent-free direct methodologies, in particular: F-BM-CL and F-BM-NO were mechanochemically synthesised via inexpensive ball

View Article Online
DOI: 10.1039/C7GC01405H

milling, whereas H-TD-E, H-TD-L, H-TD-W, and H-TD-C via alternative thermal degradation. The use of iron(III) nitrate precursor yielded magnetic composites with mixed iron oxide phases. All of the composites were found to be highly active in the microwave-assisted oxidation of isoeugenol to vanillin, with a particularly high stability after reuses of mechanochemically synthesized nanomaterials. The proposed approach proves the feasibility of producing catalytically active composites from biorefinery waste and may pave the way of a more intensive utilisation of biomass-derived waste feedstocks towards their valorisation to high added value products.

Acknowledgements

We kindly acknowledge the EU Framework Programm Horizon 2020 for financial support as in the HUGS project (ID: 675325) and project CTQ2015-68951-C3-3R (Ministerio de Economía y Competitividad, Spain and FEDER Funds). The author would also like to thank the support center SCAI of the University of Cordoba for the GC-MS analysis, Pierluigi Tosi for providing the humins foams, and María Dolores Márquez Medina for her tremendous support during the completion of this publication.

References

[1] L. Filiciotto, A.M. Balu, J.C. van der Waal, R. Luque, *Catal. Today,* 2017, DOI: 10.1016/j.cattod.2017.03.008.

[2] L. Wu, T. Moteki, A.A. Gokhale, D.W. Flaherty, F.D. Toste, *Chem.*, 2016, **1**, 32.

[3] M.J. Climent, A. Corma, S. Iborra, *Green Chem.*, 2014, **16**, 516.

[4] S. De, A.M. Balu, J.C. van der Waal, R. Luque, *ChemCatChem.*, 2015, **7**, 1608.

[5] F.D. Pileidis, M.-M. Titirici, *ChemSusChem.*, 2016, **9**, 562.

[6] M.-F. Li, S. Yang, R.-C. Sun, *Bioresour. Technol.*, 2016, **200**, 971.

[7] Avantium, (n.d.). http://www.avantium.com (accessed February 15, 2017).

[8] F.A.H. Rice, *J. Org. Chem.*, 1958, **23**, 465.

[9] T.M.C. Hoang, L. Lefferts, K. Seshan, *ChemSusChem.*, 2013, **6**, 1651.

View Article Online
DOI: 10.1039/C7GC01405H

[10] I. V. Sumerskii, S.M. Krutov, M.Y. Zarubin, *Russ. J. Appl. Chem.*, 2010, **83**, 320.

[11] I. van Zandvoort, Y. Wang, C. B. Rasrendra, E. R. H. van Eck, P. C. A. Bruijnincx, H. J. Heeres, B. M. Weckhuysen, *ChemSusChem.*, 2013, **6**, 1745.

[12] I. van Zandvoort, E.J. Koers, M. Weingarth, P.C.A. Bruijnincx, M. Baldus, B.M. Weckhuysen, *Green Chem.*, 2015, **17**, 4383.

[13] A. Mija, J.C. van der Waal, J.-M. Pin, N. Guigo, E. de Jong, *Constr. Build. Mater.*, 2017, **139**, 549-601.

[14] I. van Zandvoort, E. R. H. van Eck, P. de Peinder, H. J. Heeres, P. C. A. Bruijnincx, B. M. Weckhuysen, *ACS. Sustainable Chem. Eng.*, 2015, **3**, 533-543.

[15] S. Constant, C.S. Lancefield, B.M. Weckhuysen, P.C.A. Bruijnincx, *ACS Sustainable Chem. Eng.*, 2017, **5**, 965-972.

[16] A. Bohre, D. Gupta, M.I. Alam, R.K. Sharma, B. Saha, *ChemistrySelect*, 2017, **2**, 3129-3136.

[17] X. Tang, Y. Sun, X. Zeng, W. Hao, L. Lin, S. Liu, *Energy Fuels*, 2014, **28**, 4251.

[18] J.-P. Lange, *Angew. Chemie Int. Ed.*, 2015, **54**, 13186.

[19] T.M.C. Hoang, L. Lefferts, K. Seshan, *ChemSusChem.*, 2013, **6**, 1651.

[20] Y. Wang, S. Agarwal, A. Kloekhorst, H.J. Heeres, *ChemSusChem.*, 2016, **10**, 951.

[21] R. A. Sheldon and J. K. Kochi, *Metal Catalyzed Oxidation of Organic Compounds*, Academic Press, New York, **1981**.

[22] J.E. Bäckvall, *Modern Oxidation Methods*, Wiley–VCH, **2004**.

[23] S.M. Roberts, *Catalysts for Fine Chemical Synthesis*, Wiley–VCH, **2007**.

[24] I. Ibushi and A. Yazaki, *J. Am. Chem. Soc.*, 1981, **103**, 7371-7373.

[25] K. A. Jorgensen, *Chem. Rev.*, 1989, **89**, 431-458.

[26] R. A. Sheldon, *Green Chem.*, 2017, **19**, 18-43.

[27] D.C. Whitehead, B.R. Travis, B. Borhan, *Tetrahedron Lett.*, 2006, **47**, 3797−3800.

View Article Online
DOI: 10.1039/C7GC01405H

[28] S. Bhadra, L. Adak, *Tetrahedron Lett.*, 2008, **49**, 2588−2591.

[29] V. Kumar, V.P. Reddy, R. Sridhar, S. Srinivas, K.R. Rao, *Synlett*, 2009, **2009**, 739−742.

[30] M. Shaikh, F.-E. Hong, *Adv. Synth. Catal*. 2011, **353**, 1491−1496.

[31] K. Ghosh, P. Kumar, I. Goyal, *Inorg. Chem. Commun.*, 2012, **24**, 81−86.

[32] M.R. Maurya, N. Kumar, *J. Mol. Catal. A: Chem.* 2014, **383−384**, 172−181.

[33] H. Wójtowicz-Młochowska, *Arkivoc*, 2017, **part ii**, 12−58.

[34] G. Urgoitia, R. SanMartin, M. T. Herrero, E. Domínguez, *ACS Catal.*, 2017, **7**, 3050-3060.

[35] H. L. Liu, C. H. Soon, J. H. Wu, K. M. Lee, Y. K. Kin, *Biomaterials*, 2008, **29**, 4003-4011.

[36] M. Armand, J. M. Tarascon, *Nature*, 2008, **451**, 652-657.

[37] U. R. Pillai, E. Sahle-Demessie, V. V. Namboodiri, R. S. Varma, *Green Chem.*, 202, **4**, 495-497.

[38] A. Gonzalez-de-Castro, J. Xiao, *J. Am. Chem. Soc.*, 2015, **137**, 8206-8218.

[39] P. Tartaj, M.P. Morales, T. Gonzalez-Carreño, S. Veintemillas-Verdaguer, C.J. Serna, *Adv. Mater.*, 2011, **23**, 5243.

[40] G.S. Parkinson, *Surf. Sci. Rep.*, 2016, **71**, 272-365.

[41] Y.L. Pang, S. Lim, H.C. Ong, W.T. Chong, *Ceramics Int.*, 2016, **42**, 9.

[42] F. Arena, G. Gatti, L. Stievano, G. Martra, S. Coluccia, F. Frustreri, L. Spadaro, A. Parmaliana, *Catal. Today*, 2006, **117**, 75-79.

[43] F. Shi, M. K. Tse, M. M. Pohl, A. Bruckner, S. M. Zhang, M. Beller, *Angew. Chem., Int. Ed*., 2007, **46**, 8866–8868.

[44] K. Schröder, K. Junge, B. Bitterlich and M. Beller, *Top. Organomet. Chem.*, 2011, **33**, 83–109.

[45] M. J. Rak, M. Lerro, A. Moores, *Chem. Commun.*, 2014, **50**, 12482-12485.

[46] H. Hong, L. Hu, M. Li, J. Zheng, X. Sun, X. Lu, X. Cao, J. Lu, H. Gu, *Chem. Eur. J.*, 2011, **17**, 8726-8730.

View Article Online
DOI: 10.1039/C7GC01405H

[47] S. Perathoner, C. Centi, *Top. Catal.*, 2005, **33**, 207-224.

[48] F. Rajabi, S. Naresian, A. Primo, R. Luque, *Adv. Synth. Catal.*, 2011, **353**, 2060–2066.

[49] A. Pineda, A. M. Balu, J. M. Campelo, A. A. Romero, D. Carmona, F. Balas, J. Santamaria, R. Luque, *ChemSusChem*, 2011, **4**, 1561–1565.

[50] F. Shi, M. K. Tse, M.-M. Pohl, J. Radnik, A. Brückner, S. Zhang, M. Beller, *J. Mol. Catal. A: Chem.*, 2008, **292**, 28-35.

[51] F. Rajabi, N. Karimi, M. R. Saidi, A. Primo, R. S. Varma, R. Luque, *Adv. Synth. Catal.*, 2012, **354**, 1701-1711.

[52] M.J.W. Dignum, J. Kerler, R. Verpoorte, *Food Rev. Int.*, 2001, **17**, 199-219.

[53] C. Branzinha, D.S. Barbosa, J.G. Crespo, *Green Chem.*, **2011**, 13, 2197-2203.

[54] F. Cavani, G. Centi, in *Kirk-Othmer Encyclopedia of Chemical Technology*, vol., John Wiley & Sons, Inc., **2000**, ch. 1, pp. 1-61.

[55] M.B. Hocking, *J. Chem. Educ.*, 1997, **74**, 1055-1059.

[56] D. Hua, C. Ma, S. Lin, L. Song, Z. Deng, Z. Maomy, Z. Zhang, B. Yu, P. Xu, *J. Biotechnol.*, 2007, **130**, 463-470.

[57] S. Sanchez, A. L. Demain, *Org. Process Res. Dev.*, 2010, **15**, 224-230.

[58] K. Li, J. Frost, *J. Am. Chem. Soc.*, 1998, **120**, 10545-10546.

[59] J. Lawless, *The Encyclopedia of Essential Oils*, Thorsons, London, UK, **2002**, p. 48-168.

[60] N. Wangrangsimagul, K. Klinsakul, A. S. Vangnai, J. Wongkongkatep, P. Inprakhon, K. Honda, H. Ohtake, J. Kato, T. Pongtharangkul *Appl. Microbiol. Biotechnol.*, 2012, **93**, 555-563.

[61] M. Tan, S. L. Liew, M. Y. Maskat, W. A. W. Mustapha, O. Hassan *Int. Food Res. J.*, 2015, **22**, 1651-1656.

[62] H. Kawamoto, in *Production of Biofuels and Chemicals from Lignin*, ed. Z. Fang and R.L. Smith Jr., Springer, **2016**, ch. 11, pp. 321-354.

[63] W.A. Herrmann, T. Weskamp, J.P. Zoller, R.W. Fischer, *J. Mol. Catal. A: Chem.*, 2000, **153**, 49-52.

View Article Online
DOI: 10.1039/C7GC01405H

[64] E.V. Gusevskaya, L. Menini, L.A. Parreira, R.A. Mesquita, Y.N. Kozlov, G.B. Shul'pin, *J. Mol. Catal. A: Chem.*, 2012, **363-364**, 140-147.

[65] I.B. Adilina, T. Hara, N. Ichikuni, S. Shimazu, *J. Mol. Catal. A: Chem.*, 2012, **361-362**, 72-79.

[66] P.T. Anastas and J.C. Warner, *Green Chemistry: Theory and Practice*, Oxford University Press, New York, **1998**, pp. 30.

[67] C. Xu, S. De, A.M. Balu, M. Ojeda, R. Luque, *Chem. Commun.*, 2015, **51**, 6698-6713.

[68] Avantium Knowledge Centre B.V., WO Pat., WO2017074183 (A8), **2017**.

[69] M. Ojeda, A.M. Balu, V. Barron, A. Pineda, A. Garcia, A.A. Romero, R. Luque, *J. Mater. Chem A*, 2014, **2**, 387-393.

[70] D. Hua, C. Mab, S. Lin, L. Song, X. Denga, Z. Maomy, Z. Zhang, B. Yu, P. Xu, *J. Biotechnol.*, 2007, **130**, 463-470

[71] Y. Zhang, P. Xu, S. Han, C. Ma, *Appl. Microbiol. Biotechnol.*, 2006, **73**, 771-779.

[72] R. S. Ribeiro, A.M.T. Silva, J.L. Figueiredo, J.L. Faria, H.T. Gomes, *Carbon*, 2013, **62**, 97-108.

[73] M. Hermanek, R. Zboril, I. Medrik, J. Pechousek, C. Gregor, *J. Am. Chem. Soc.*, 2007, **129**, 10929-10936.

[74] M. Gurol and S. Lin, *J. Adv. Oxid. Technol.*, 2002, **5**, 147-154.